



S0092-8240(97)00025-6

PHASE TRANSITION FROM ENVIRONMENTAL TO DYNAMIC DETERMINISM IN MOUNTAIN PINE BEETLE ATTACK

■ PETER WHITE and JAMES POWELL
Department of Mathematics and Statistics,
Utah State University,
Logan, UT 84322-3900, U.S.A.

(E.mail: pwhite, powell@sunfs.math.usu.edu)

Mountain pine beetle outbreaks are responsible for widespread tree mortality in pine forests throughout western North America. Intensive outbreaks result in significant economic loss to the timber industry and massive changes to the forest habitat. Because of the time and space scales involved in a beetle outbreak, mathematical models are needed to study the evolution of an outbreak. In this paper we present a partial differential equation model of the flight phase of the mountain pine beetle which includes chemotactic responses and tree defense. We present a numerical method for integrating this model and use this method to investigate the relationship between emergence rate, forest demographics and patterns of beetle attack. In particular we look at how emergence rate affects the beetles' ability to successfully attack strong trees, which may be an indicator of an epidemic outbreak.
© 1997 Society for Mathematical Biology

1. Introduction. The interaction between mountain pine beetles (MPB, *Dendroctonus ponderosae* Hopkins) and pine tree hosts (in particular, lodgepole, *Pinus contorta*, and ponderosa, *Pinus ponderosae*) is the backdrop for some of the best current questions in mathematical biology, disturbance ecology and biological management. MPB has long been considered a major pest in western forests. As an aggressive bark beetle (one that kills its host), eruptions of this species are impressive events. Outbreaks can be both intensive (up to 80% or greater mortality) and extensive (covering thousands of contiguous acres), resulting in serious economic consequences. It is also becoming recognized that disturbances, such as MPB outbreaks, may be central to maintaining the structure, function and health of western forests. At endemic levels, MPB maintain a presence in pine forests over many years, infesting weak trees as wolves select aged and diseased caribou. When population densities become high enough, infestations reach epidemic levels capable of killing many acres of vigorous, healthy trees. The transition between these states, mechanism of selection, role of environmental and dynamic determinism in MPB dispersal and ecological interaction between MPB dispersal, fire and management is only vaguely understood.

The ecosystem itself presents many challenges to traditional observational or experimental understanding. The landscapes are physically challenging, with scales large enough to disallow casual observation. Multiple time scales complicate understanding; dispersal occurs for only a few weeks out of each year, yet individual events of infestation wax and wane over one or two days. Consequently, thorough understanding of spatial events requires detailed observation at many sites over several weeks, and yet spatial patterns may only evolve after several years. The physical scale of the hosts prohibits laboratory experimentation, while the status of western pine forest as timber and recreational resources complicates on-site experimentation. Mathematical modeling and simulation techniques therefore provide an important alternative mechanism for understanding.

The landscape in mathematical biology is not without its challenges, however. The most natural mathematical language to describe spatio-temporal population dispersal involves partial differential equations (PDE). The complicated interaction between MPB, host and chemical landscape requires non-linear descriptions, at which point one leaves the safe haven of known equations and solutions and enters unknown territory. This paper is centered around analyzing the mathematical description of MPB dispersal using computational and analytic approaches.

The state of the modeling and our approaches to the mathematical challenges will be described in the next few sections. The picture which emerges from these investigations is striking: the biological switch between endemic and epidemic levels of infestation represents a transition from environmental to dynamic determinism in the mathematical model. In the environmentally dominated regime, populations are only large enough to establish themselves in "weak" hosts. The spatial pattern of attack and MPB dispersal is determined primarily by the effects of environment on host. As populations grow large enough, the locus of primary attacks continues to be determined by the environment. However, primary attacks serve to focus surplus population, which can reach high enough densities to successfully infest "strong," secondary hosts. This is manifested as a loss in spatial correlation between host vigor and successful attacks, which will be discussed below.

2. The MPB Dispersal Model

2.1. *Behavior of the pine beetle /host tree system.* Because of its economic impact, MPB population dynamics has been the subject of sustained research efforts dating from the early 1900s, focussed primarily on protection of valuable forest resources. Although this insect spends most of its life cycle under the bark feeding on phloem tissue, the relatively short phase of the life cycle in which emergence and attack of new hosts occurs is essential

for continuing the population. It is during this time that complex spatial dynamics come into play.

The MPB is typically a univoltine species which attacks living pines. Unlike most phytophagous insects, successful reproduction is contingent upon death of all or part of the host (Sheppard, 1966, Wood, 1972). Host trees, however, have evolved effective response mechanisms to defend themselves against bark beetle attacks (Smith, 1963, 1966; Reid *et al.*, 1967; Nebeker *et al.*, 1993; Raffa *et al.*, 1993). Almost all trees are capable of responding to bark beetle attacks, but only those with a rapid and sustained reaction are likely to survive. If many beetles attack the same tree over a short period of time (e.g., mass attack), they can exhaust the tree's defensive mechanisms. The final outcome of a bark beetle dispersal and colonization attempt is, therefore, dependent upon a series of competing rate reactions which regulate both beetle arrival and host response (Raffa and Berryman, 1979; Safranyik *et al.*, 1989).

The evolved relationship between the MPB and its host trees has resulted in an elaborate chemical communication system. Through a chemically mediated synergistic reaction with host chemical compounds, female beetles attacking a tree release trans-verbenol, which, when mixed with α -pinene, is an aggregation pheromone attracting both sexes (Pitman, 1971; Pitman *et al.*, 1968; Hughes, 1973). At higher concentrations of trans-verbenol, higher proportions of males are attracted (Renwick and Vite, 1970). Attacking males produce exo-brevicomin, which at low concentrations primarily attracts females (Conn *et al.*, 1983). This system of chemical communication results in mass attack on a single focus tree. However, the tree is a finite food resource that can be overexploited by too many beetles. Verbenone, an epidietic¹ pheromone, is released by attacking males and inhibits the landing of additional beetles at high concentrations (Borden *et al.*, 1987). Once the concentration of verbenone sufficiently exceeds the concentration of aggregating pheromones, flying beetles in the area switch to nearby host trees (McCambridge, 1967; Geizler and Gara, 1978; Geizler *et al.*, 1980). When the incoming beetles switch, the new tree often has greater attack rates and is colonized more rapidly than the original focus tree (Rasmussen, 1974). The switching mechanism provides a means for efficiently utilizing the available population of attacking beetles.

Although density-dependent beetle-produced pheromone responses play the dominant role in organizing MPB attacks, kairomones produced by the tree may also play a part (Hunt *et al.*, 1989). At low population densities, attacking MPB selectively attack trees weakened by disease or other stresses (Tkacz and Schmitz, 1986; Schmitz, 1988; Schowalter and Filep, 1993). It is hypothesized that stressed trees release a kairomone signal

¹The term epidietic describes specific sorts of animal behavior which are used principally for population density regulation (Prokopy, 1980).

which attracts MPB flying in the vicinity, providing primary attraction to a particular tree (Gara *et al.*, 1984; Moeck and Simmons, 1991, Roe and Amman, 1970). An alternative hypothesis is that new hosts are found using a combination of random landings guided by visual cues (Schonherr, 1976; Sheppard, 1966), followed by chemical and tactile cues once on the host tree (Hynum and Berryman, 1980; Raffa and Berryman, 1979). Most likely, both situations occur. Although the combination of factors that signals a weakened tree remains an open question, enough evidence exists for the effect of host compounds on beetle behavior (Norris and Baker, 1967; Raffa and Berryman, 1982; Raffa, 1988) that models of MPB spatial dynamics should include some representation of host volatiles, as well as beetle-produced pheromones.

The complex chemical cues in the MPB/pine tree interaction act as self-focussing and self-dissipating forces. The interaction of these forces results in a non-linear density-dependent response and creates complex spatial patterns of resource utilization. Although the explicit spatial feedback is critical to the ecological association of MPB with its hosts, there is no spatially explicit model of the interaction before our work (Powell *et al.*, 1995; Powell and Rose, 1996; White and Powell, 1996). In the next section we will review the construction of a spatio-temporal PDE model of the MPB/host spatial ecology.

2.2. *The global model.* We define the following variables, which depend on spatial location, x , y and time, t :

- $P(x, y, t)$ population of flying MPB
- $Q(x, y, t)$ population of (alive) nesting/eating MPB
- $A(x, y, t)$ concentration of pheromones
- $C(x, y, t)$ concentration of volatiles released by attacked trees
- $S(x, y, t)$ resin outflow
- $R(x, y, t)$ resin capacity (related to phloem thickness and size of tree)
- $H(x, y, t)$ number of entrance holes bored by attacking MPB

If we neglect spatial redistribution, the number of flying MPB decreases proportionally to the death rate, $\omega_1 P$, and the number of beetles landing and nesting in a tree, $r_1(R/R_0)P(1 + \sigma A)$. The term $r_1 P$ captures randomly landing MPB; the term $r_1 \sigma A P$ describes the nesting in response to attractant aerosols. R_0 is the rest resin capacity of the tree, which is proportional to the surface area of the bole. Consequently, the fraction R/R_0 measures the uninfested portion of the bole. This gives a dynamic equation for changes in flying MPB density:

$$\dot{P} = -\omega_1 P - r_1 \frac{R}{R_0} P(1 + \sigma A) + \gamma.$$

The term γ is the emergence rate of flying MPB.

The nesting population, Q , grows proportionally to $r_1 P(1 + \sigma A)$. Nesting MPB die at some rate, $\omega_2 Q$. Finally, beetles may be killed by the natural defense mechanisms of the host-resin outflow. The population of nesting MPB should decrease in proportion to the resin outflow through occupied burrows, $\beta_1 S(Q/H)$. This gives an equation for Q ,

$$\dot{Q} = -\omega_2 Q + r_1 \frac{R}{R_0} P(1 + \sigma A) - \beta_1 S \frac{Q}{H}. \quad (1)$$

The rate of increase in the number of holes drilled is precisely equal to the number of MPB who have attempted to nest. On the other hand, resin crystallizes after flowing through burrows, slowly closing the hole. This means that holes should be lost at a rate proportional to the amount of resin outflow, S , which itself is proportional to the number of holes and the available resin capacity,

$$S = r_3 HR.$$

A rate equation for H is then given by

$$\dot{H} = r_1 \frac{R}{R_0} P(1 + \sigma A) - r_4 r_3 HR. \quad (2)$$

It remains to be determined how the local resin capacity and the amount of resin outflow vary with time. Let R_0 be the reservoir capacity the tree would maintain naturally. When $R \rightarrow 0$ the tree has no capacity to replenish its reservoir, so that the rate of change of the resin capacity should be proportional to $R(R_0 - R)$. Resin capacity is depleted proportionally to the number of entrance holes and the available amount of resin which can flow out through the holes. These two processes give

$$\dot{R} = [r_2(R_0 - R) - r_3 H] R. \quad (3)$$

This set of equations reflects the temporal behavior without spatial redistribution. We resolve spatial redistribution by considering the effect of various "fluxes" on the population density. Denote the flux vector by Φ . There are three basic components to the flux function, reflecting the beetles' recognition of potential hosts, their response to pheromones and the degree of randomness in their behavior. Thus,

$$\Phi = \phi_C + \phi_A + \phi_P,$$

where:

- ϕ_C is flux along gradients of $C(x, y, t)$ due to chemotactic recognition of potential hosts,

$$\phi_C = \kappa P \nabla C.$$

- Φ_A is flux due to the beetles' attraction to/repulsion from the suite of pheromones, A . The summed response of these pheromones is attractive in small concentrations, repulsive in larger concentrations, giving

$$\Phi_A = \nu P \frac{A_0 - A}{A_0 + A/A_3} \nabla A = \nu P \nabla f(A),$$

where

$$f(A) = A_3 \left\{ A_0 (A_3 + 1) \ln \left[1 + \frac{A}{A_3 A_0} \right] - A \right\}.$$

This flux function has the effect of attracting MPB for small A , but with saturable repulsive effect (parametrized by A_3) for $A > A_0$.

- Φ_P is flux due to the beetles' random redistribution in the absence of other influences, dependent only on spatial changes in the density of flying beetles, which gives

$$\Phi_P = -\mu \nabla P.$$

Adding the effects of these fluxes gives a spatio-temporal evolution equation for P ,

$$\begin{aligned} \frac{\partial}{\partial t} P = & -\nabla \cdot \{ [\kappa \nabla C + \nu \nabla f(A)] P - \mu \nabla P \} \\ & - \omega_1 P - r_1 \frac{R}{R_0} P (1 + \sigma A) + \gamma. \end{aligned} \quad (4)$$

We will assume that the chemical concentrations, A and C , obey standard diffusion laws, but with sources and sinks of their own. For the suite of pheromones released by nesting beetles, sources are proportional to Q , while losses occur due to chemical decomposition. These effects give a linear diffusion equation for A ,

$$\frac{\partial}{\partial t} A = b_1 \nabla^2 A + a_1 Q - \delta_1 A. \quad (5)$$

For host kairomones, C , the source is resin outflow. Again, we expect some loss due to chemical decomposition, given an equation similar to that for A ,

$$\frac{\partial}{\partial t} C = b_2 \nabla^2 C + a_2 S - \delta_2 C. \quad (6)$$

Table 1. The list of parameters appearing in the global PDE model for MPB redistribution

Parameter	Description
κ	A measure of the beetles' perception of and attraction to weakened pines
ν	Attractiveness of pheromones
μ	Diffusivity of flying beetle population due to randomness
A_0	Critical concentration at which pheromone becomes repulsive
A_3	Saturation parameter for pheromone
a_1	Rate of pheromone creation by burrowing beetles
b_1	Rate of pheromone diffusion
δ_1	Loss rate of pheromone
a_2	Rate of kairomone creation by host tree
b_2	Rate of kairomone diffusion
δ_2	Loss rate of kairomone
R_0	Local peak resin capacity
σ	Rate of directed infestation
r_1	Rate of sampling infestation
r_2	Rate of resin replenishment
r_3	Rate of resin outflow through burrows
r_4	Rate of resin crystallization
ω_1	Death rate of airborne beetles
ω_2	Death rate of nesting beetles
β	Rate at which trees' natural defenses kill nesting beetles
$\gamma(t)$	Emergence rate of new populations of airborne beetles (not constant)

Equations (1)–(6) are a complete spatio-temporal description of the dependent variables controlling the behavior of MPB/pine relationship. The number of free parameters—a measure of the descriptive degrees freedom—is given in Table 1.

3. Numerical Method. Equations (1)–(6) are coupled, non-linear reaction–diffusion PDE. Other than the fact that solutions exist for finite times and sensible initial conditions, mathematics offers no theory regarding the solution of such equations. The most natural way to solve these equations is to attempt a numerical solution by discretizing space and solving the resulting ordinary differential equations (ODE). To achieve sufficient resolution on a multi-kilometer landscape requires tens or hundreds of thousands of spatial nodes, with a system of non-linear equations to be solved at each node. As if this did not represent enough complication, the equations are stiff because of the variety of temporal scales in the parameters (see Table 2) which we estimated in Powell *et al.* (1995). Consequently, even approximate solution of the governing equations has been a challenge (White and Powell, 1996). We have chosen to use the variety of scales to our advantage, solving the fastest, equations (5) and (6), analytically. This allows us to use a straightforward explicit numerical method on the remaining four equations.

Table 2. Parametric values for numerical simulation and units^a

Parameter	Value	Units
a_1	400	$\text{tmg hec}^{-1} \text{fh}^{-1} \text{MPB}^{-1}$
b_1	50	hec fh^{-1}
δ_1	200	fh^{-1}
A_0	2	tmg hec^{-1}
μ	1.	hec fh^{-1}
ω_1	0.1	fh^{-1}
σ	15	hec tmg^{-1}
r_1	0.15513	fh^{-1}
r_3	0.025	fh^{-1}
R_0	Mean of 1	R_0
A_3	0.2	—
a_2	400	$\text{tmg hec}^{-1} \text{fh}^{-1}$
b_2	50	hec fh^{-1}
δ_2	200	fh^{-1}
ν	10	$\text{hec}^3 \text{tmg}^{-2} \text{fh}^{-1}$
κ	8	$\text{hec}^2 \text{tmg}^{-1} \text{fh}^{-1}$
ω_2	0.001	fh^{-1}
β	100	$\text{MPB } R_0^{-1}$
r_2	0.05	$R_0^{-1} \text{fh}^{-1}$
r_4	0.1	$R_0^{-1} \text{fh}^{-1}$
ρ	2	$\text{hec}^{1/2}$
$\gamma(t)$	—	$\text{MPB hec}^{-1} \text{fh}^{-1}$

^aUnits involving resin are measured relative to R_0 . We have used fh as an abbreviation for flight hour, hec for hectare and tmg for tens of micrograms.

We discretize the space domain and approximate the continuous PDEs with a system of ordinary differential equations (ODE) of the state variables in time. Because we are interested in comparing patterns of successful attacks when varying parameters, we may assume periodic boundary conditions and use spectral methods for calculating spatial derivatives, as explained below. For the chemical equations we solve the ODEs analytically in Fourier space. For equations (1)–(4) we use an Adams variables step predictor–corrector method.

3.1. *Spectral derivatives.* Consider the periodic function, $f(x)$, with period $2L$. If f is suitably differentiable, then f can be written as a Fourier series

$$f(x) = \sum_{l=-\infty}^{\infty} \hat{f}_l \exp\left(\frac{il\pi x}{L}\right)$$

and

$$f'(x) = \sum_{l=-\infty}^{\infty} \frac{il\pi}{L} \hat{f}_l \exp\left(\frac{il\pi x}{L}\right),$$

where $i = \sqrt{-1}$ and \hat{f}_j are the Fourier coefficients of f . Here differentiation in the state space, x , corresponds to multiplication in Fourier space. This process can be extended to functions of two variables to get

$$f(x, y) = \sum_{l=-\infty}^{\infty} \sum_{m=-\infty}^{\infty} \hat{f}_{lm} \exp\left(\frac{il\pi x}{L_x} + \frac{im\pi y}{L_y}\right),$$

where $f(x, y) = f(x + 2L_x, y + 2L_y)$ and \hat{f}_{lm} are the Fourier coefficients.

In our numerical method we discretize the space domain into n_x by n_y grid points so that $\Delta x = 2L_x/n_x$, $\Delta y = 2L_y/n_y$, $x_j = -L_x + j\Delta x$ and $y_k = -L_y + k\Delta y$. In this setting we can approximate $f(x_j, y_k)$ by a finite series

$$f(x_j, y_k) = f_{jk} = \sum_{l=-n_x/2}^{n_x/2-1} \sum_{m=-n_y/2}^{n_y/2-1} \hat{f}_{lm} \exp\left(\frac{il\pi x_j}{L_x} + \frac{im\pi y_k}{L_y}\right)$$

of the n_x by n_y Fourier modes, where we choose n_x and n_y to be powers of 2 for convenience. Then the approximations to the space derivatives are found by calculating the Fourier coefficients (transforming from state space to Fourier space), \hat{f}_{lm} , multiplying these coefficients by the corresponding constant, $il\pi/L_x$ or $im\pi/L_y$ which are the eigenvalues of the matrix approximations to the derivative operators $\partial/\partial x$ and $\partial/\partial y$, and then transforming back to state space via a summation. Transforming between state space and Fourier space can be accomplished using discrete fast Fourier transforms² with $\mathcal{O}((n_x \log n_x)(n_y \log n_y))$ floating point multiplications if n_x and n_y are chosen to be powers of 2.

3.2. Semi-analytic solution for the chemical equations. In our discretized space, the evolution of the chemicals is governed by the ordinary differential equations

$$\frac{d}{dt} A_{jk} = b_1(\Delta A)_{jk} + a_1 Q_{jk} - \delta_1 A_{jk} \quad (7)$$

and

$$\frac{d}{dt} C_{jk} = b_2(\Delta C)_{jk} + a_2 r_3 H_{jk} R_{jk} - \delta_2 C_{jk}. \quad (8)$$

In Fourier space these equations become

$$\frac{d}{dt} \hat{A}_{lm} = (b_1 D_{lm} - \delta_1) \hat{A}_{lm} + a_1 \hat{Q}_{lm}$$

²We use the optimized FFT packages from the netlib@ornl.gov archive.

and

$$\frac{d}{dt} \hat{C}_{lm} = (b_2 D_{lm} - \delta_2) \hat{C}_{lm} + a_2 r_3 \widehat{HR}_{lm},$$

where D_{lm} is the appropriate multiple for the Fourier derivatives. Each of these equations in Fourier space has the form

$$y' = \alpha y + k,$$

where α is a constant and k is a function of t and has solutions satisfying

$$y(t + \Delta t) = e^{\alpha \Delta t} y(t) + e^{\alpha \Delta t} \int_t^{t + \Delta t} e^{-\alpha(t-\tau)} k(\tau) d\tau.$$

If we assume that k is nearly constant on the interval $[t, t + \Delta t]$, an assumption justified by the rapidity of chemical evolution, then

$$y(t + \Delta t) \approx e^{\alpha \Delta t} y(t) + \frac{e^{\alpha \Delta t} - 1}{\alpha} k. \quad (9)$$

Since Q , H and R evolve at a much slower rate than the chemicals, we can treat them as constants over short time intervals and solve the chemical equations exactly up to the number of Fourier modes included. For equation (7) we calculate the Fourier coefficients of A and Q at time t , then advance the solution in Fourier space to time $t + \Delta t$ using (9) and finally transform the solution back to state space using an inverse Fourier transform. A similar process is used to advance (8).

3.3. Discretization of non-chemical equations. For convenience of notation we reduce our model to one space dimension, x , and note that the following can be extended to two dimensions in a straightforward manner. Since we are interested in the change of attack patterns, we may assume periodic spatial boundary conditions and use the Fourier differentiation methods discussed earlier in approximating the space derivatives. If \mathcal{F} represents this approximation of the derivative operator,

$$\frac{dA}{dx}(x_j) \approx (\mathcal{F}A)_j = \sum_{l=-n/2}^{n/2-1} \hat{A}_l \frac{il\pi}{L} \exp\left(\frac{il\pi x_j}{L}\right),$$

then the discrete approximations for equations (1)–(4) are

$$\begin{aligned} \frac{d}{dt}Q_j &= r_1P_i(1 + \sigma A_j)\frac{R_j}{R_{0j}} - \omega_2Q_j - \beta Q_jR_j, \\ \frac{d}{dt}H_j &= r_1P_j(1 + \sigma A_j)\frac{R_j}{R_{0j}} - r_4H_jR_j, \\ \frac{d}{dt}R_j &= [r_2(R_{0j} - R_j) - r_3H_j]R_j. \\ \frac{d}{dt}P_j &= -(\mathcal{F}\Phi)_j - r_1P_j(1 + \sigma A_j)\frac{R_j}{R_{0j}} - \omega_1P_j + f_j(t), \\ \Phi_j &= \left[\kappa(\mathcal{F}C)_j + \nu\frac{a_0 - A_j}{a_0 + A_j/A_3}(\mathcal{F}A)_j \right]P_j - \mu(\mathcal{F}P)_j. \end{aligned}$$

This results in a pseudo-spectral method for solving the PDE numerically.

3.4. *Numerical technique.* For the above system of equations we chose to use a standard Adams–Bashforth–Moulton fourth-order predictor–corrector algorithm with a variable step size. We chose this method for ease of programmability (Burden and Faires, 1985), stability properties in a ODE setting (Gear, 1991) and the flexibility of self-correcting step sizes. This last consideration was important because of the large differences in the magnitudes of the coefficients in the MPB model, which combined with the aggregating non-linearity, produces sporadic spatial stiffness.

To summarize the method, consider the system of differential equations

$$\frac{d}{dt}\mathbf{v} = \mathbf{F}(\mathbf{v}, t), \quad \mathbf{v}(t_0) = \mathbf{v}^{(0)},$$

where $\mathbf{v}(t)$ is a vector-valued function of t . If we denote $\mathbf{v}^{(i)} = \mathbf{v}(t_0 + ih)$, where h is the time step, then the Adams method can be written in the form

$$\begin{aligned} \mathbf{w}_p^{(i+1)} &= \mathbf{v}^{(i)} + \frac{h}{24} [55\mathbf{F}(\mathbf{v}^{(i)}, t^{(i)}) - 59\mathbf{F}(\mathbf{v}^{(i-1)}, t^{(i-1)}) \\ &\quad + 37\mathbf{F}(\mathbf{v}^{(i-2)}, t^{(i-2)}) - 9\mathbf{F}(\mathbf{v}^{(i-3)}, t^{(i-3)})], \\ \mathbf{w}_c^{(i+1)} &= \mathbf{v}^{(i)} + \frac{h}{24} [9\mathbf{F}(\mathbf{w}_p^{(i+1)}, t^{(i+1)}) + 19\mathbf{F}(\mathbf{v}^{(i)}, t^{(i)}) \\ &\quad - 5\mathbf{F}(\mathbf{v}^{(i-1)}, t^{(i-1)}) + \mathbf{F}(\mathbf{v}^{(i-2)}, t^{(i-2)})], \end{aligned}$$

where $\mathbf{w}_p^{(i+1)}$ is a predictor for $\mathbf{v}^{(i+1)}$ and $\mathbf{w}_c^{(i+1)}$ is a corrector for $\mathbf{v}^{(i+1)}$. At each step an error estimate in the approximation is calculated using the predictor and corrector. A weighted difference of the form

$$\delta = \max \frac{|\mathbf{w}_c^{(i+1)}(j) - \mathbf{w}_p^{(i+1)}(j)|}{1 + |\mathbf{w}_c^{(i+1)}(j)|}$$

is calculated. Then an estimate of the error (see Burden and Faires, 1985) is given by

$$\text{error} = \frac{19\delta}{270h}.$$

If this error is less than a user supplied tolerance then we set $\mathbf{v}^{(i+1)} = \mathbf{w}_c^{(i+1)}$ and move on the next time step. If the error is found to be too large, then $\mathbf{w}_p^{(i+1)}$ and $\mathbf{w}_c^{(i+1)}$ are recalculated using a smaller value of h . If the error is much less than the tolerance, then the step size is increased for the next time step. Each time the step size is changed it is necessary to calculate three “starter” values needed by the predictor and corrector. To calculate these starter values we used a standard fourth-order Runge–Kutta method (Press *et al.*, 1992).

These are several advantages to using an Adams variable step method. Given the values of $\mathbf{F}(\mathbf{v}^{(j)}, t^{(j)})$ for $j = i - 3, i - 2, i - 1$, which can be saved from previous steps, only two evaluations of \mathbf{F} are needed for this fourth-order method. Using information about the solution at four previous time steps gives better stability than standard methods which do not need this information. The method chooses the appropriate time step instead of requiring the user to supply that information. Finally, the corrector step corresponds to doing one iteration of an implicit solution of the system, which tends to be more efficient for solving stiff problems than explicit methods. The disadvantages of using the Adams variable step size method include need for storage space for past information and the necessity of small time steps. An added burden is the computational overhead involved in detecting the need to change step size and the calculation of the starter values.

4. Results. We have used the above numerical method to investigate the role of environmental determinism in the dynamic MPB model. The “parameter” R_0 is the reservoir resin capacity of an individual tree and is a surrogate for tree vigor and health. Tree phloem is responsible for carrying the storing resin and is the target region for MPB infestation. Since the phloem lies just under the bark, R_0 is a measure of bole surface area and phloem thickness. Within flight season the major source of environmental variation in the model is spatial heterogeneity in R_0 , reflecting forest demographics.

We have run the model using a randomly selected forest with R_0 varying uniformly from 0.5 to 1.5, and tested the response of the model at various levels of emergence, γ , from 5 to 20 MPB/(hectare-flight hour). We performed the simulations with chemotaxis and without chemotaxis ($\nu = \kappa = 0$) to compare attack patterns under dynamic determinism and environmental determinism. By setting ν and κ to zero we model MPB movement only caused by random dispersion, meaning that any patterns observed are the result of environmental heterogeneity. Non-chemotactice runs are used as a “baseline” to check pattern formation in our model against patterns generated in the absence of chemical cues.

Since the phloem is the food source for the MPB larvae, a healthy tree with large R_0 would represent a “tasty” target of attack from a reproductive perspective. However, a healthy tree’s defensive capabilities would require a greater focus of attack to achieve sufficient numbers of MPB to overwhelm the tree. At relatively low levels of emergence there are insufficient numbers of beetles to successfully target healthy trees. In this case, only the weak trees can be infested and we should see attack pattern influenced largely by forest demographics or what we are calling environment determinism. At higher rates of emergence, the weak trees serve as focal points, but the MPB densities are great enough so that secondary attacks on nearby trees of arbitrary health are also successful. This then causes a cascade effect which draws in more flying MPB from the surrounding area and creates more secondary attacks, resulting in areas of successful infestation regardless of forest demographics.

This switchover from primary to secondary attacks can be seen in our PDE model in Figures 1 and 2. In Fig. 1 we show the resulting forest health and beetle attack patterns after 40 flight hours at emergence levels of 7.5 MPB/(hectare-flight hour) in parts (a) and (b) and 10 MPB/(hectare-flight hour) in parts (c) and (d). Figure 1(a) and (c) are without chemotaxis, while Fig. 1(b) and (d) are with chemotaxis. In Fig. 2 the resulting attack patterns are shown for levels of emergence of 12.5 and 15 MPB/(hectare-flight hour). In the absence of chemically directed movement the only pattern formation is in the form of survival of the fittest trees, where the MPB are only able to successfully attack the weak trees. When including chemotaxis there is a marked switching in attack patterns with more organization on the part of the flying MPB at higher rates of emergence.

From Figs. 1 and 2 we can conclude that in the presence of chemotaxis either the bulk number of beetles emerging or the rate of emergence is key to secondary attack success. To see that the rate of emergence is the cause of the pattern formation and not the bulk number of beetles emerging, we ran simulations varying the time over which a fixed number of beetles emerged. In Figs. 3 and 4 we see that the beetles achieve a better focus of attack at the higher emergence rate, Fig. 3(a), and that as the emergence rate decreases so does the beetles’ ability to organize their attack. Thus, the

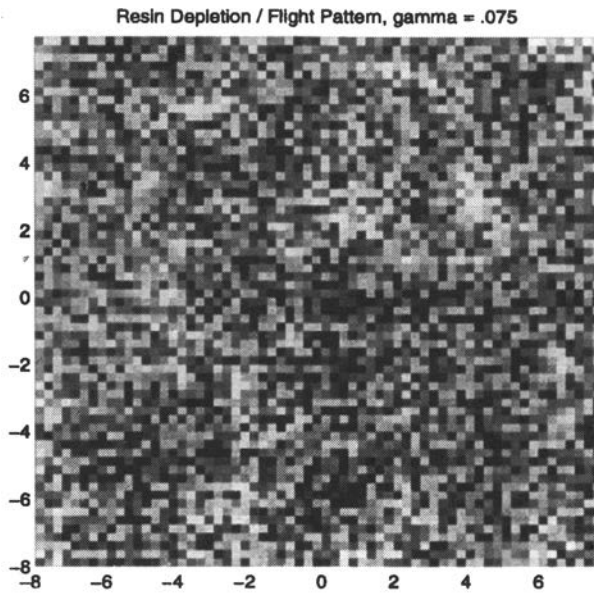
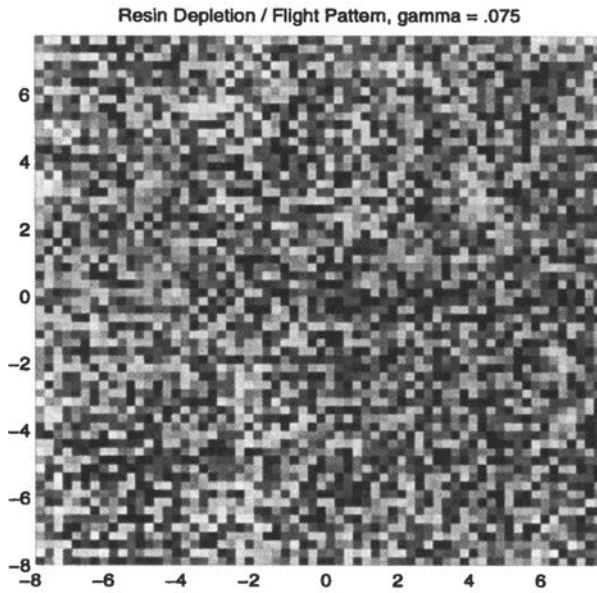
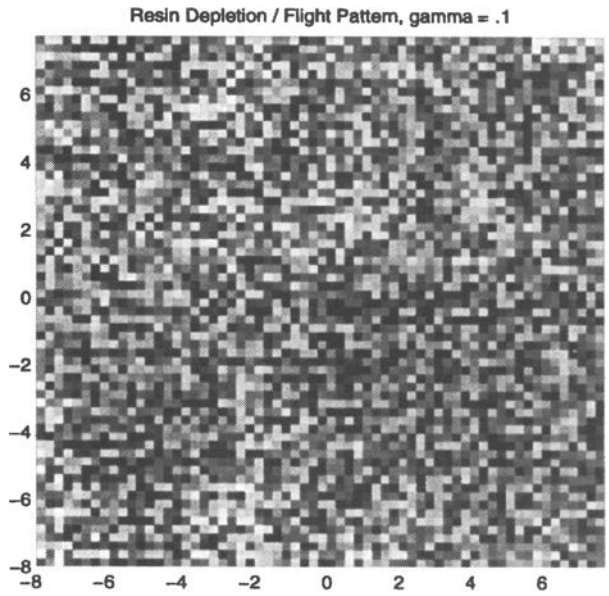
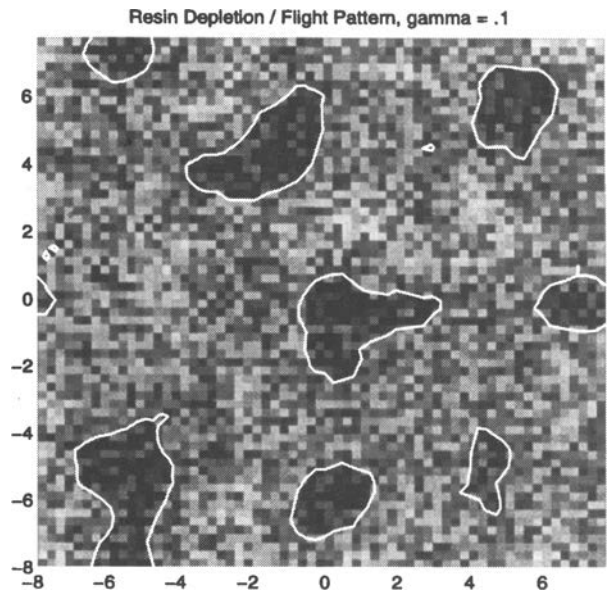


Figure 1. Forest health/beetle attack patterns both with chemotaxis (b and d) and without chemotaxis (a and c) after 40 flight hours at emergence levels of 7.5 and 10 MPB/(hectare-flight hour). Dark grey denotes low resin (poor health); contour lines show varying densities of flying MPB.



(c)



(d)

Figure 1. (Continued).

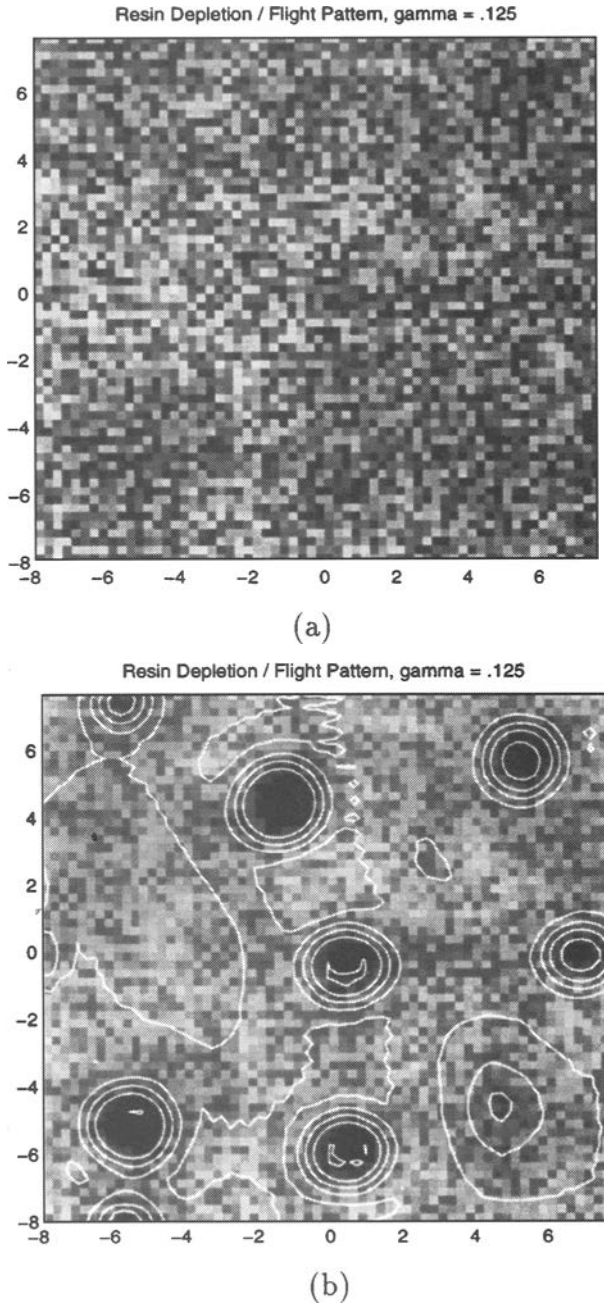
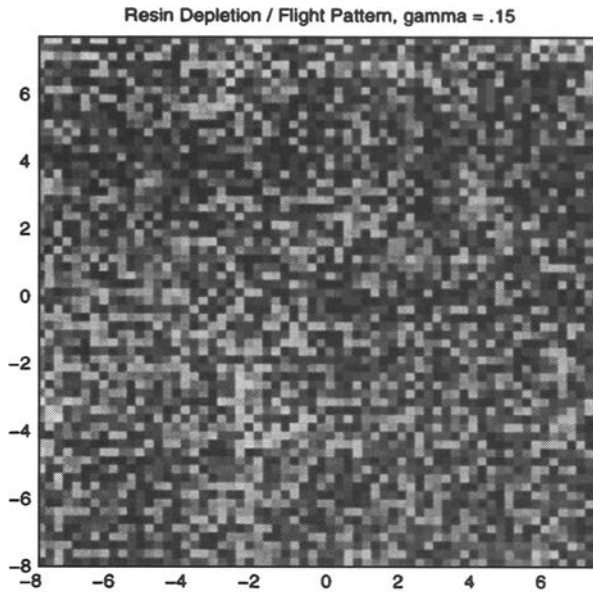
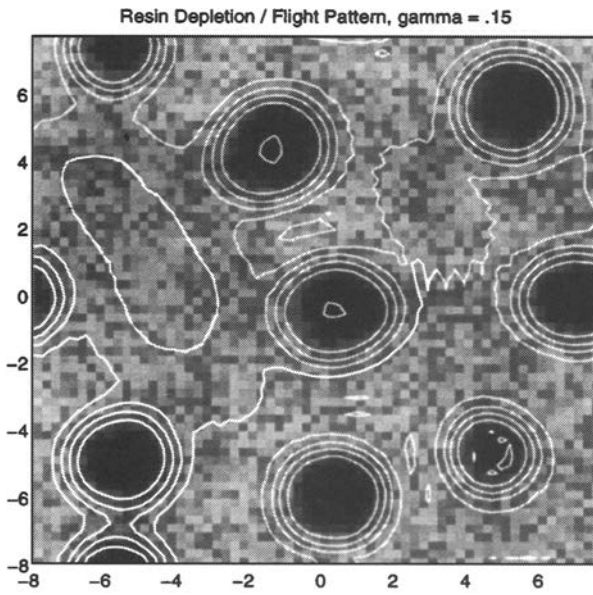


Figure 2. Forest health/beetle attack patterns both with chemotaxis (b and d) and without chemotaxis (a and c) after 40 flight hours at emergence levels of 12.5 and 15 MPB/(hectare-flight hour). Dark grey denotes low resin (poor health); contour lines show varying densities of flying MPB.

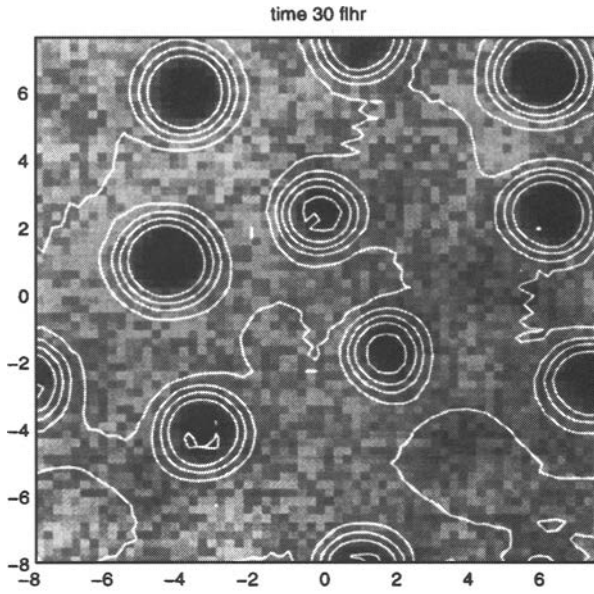


(c)

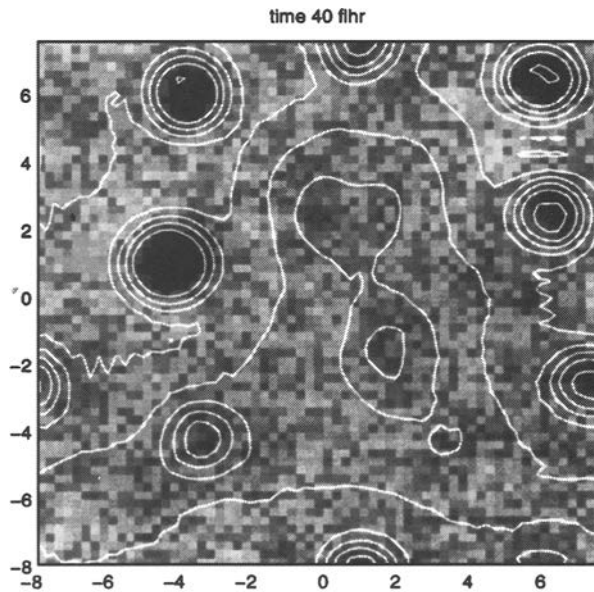


(d)

Figure 2. (Continued).

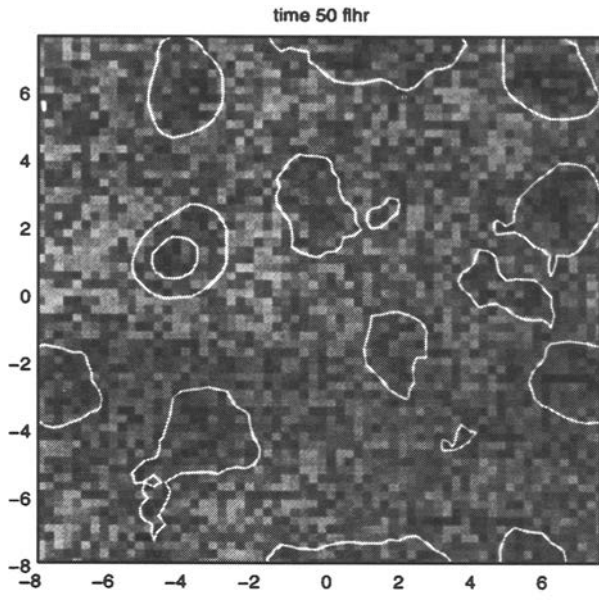


(a)

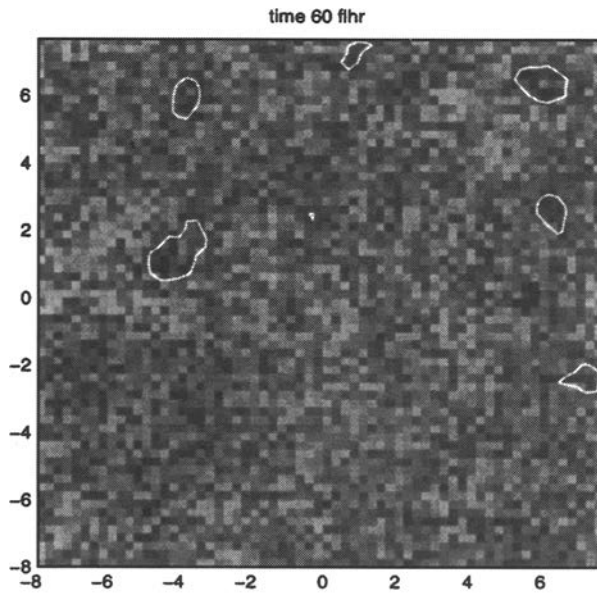


(b)

Figure 3. Tree health/MPB flight pattern on inhomogeneous forest with the same number of beetles emerging over 30, 40, 50 and 60 flight hours. Frame (a) shows the demographics of the forest when emergence occurs over a 30 flight hours period; light grey denotes high resin levels (good health); dark grey denotes lower resin level (poor health); contour lines represent different level of density of flying MPB.



(c)



(d)

Figure 3. (Continued).

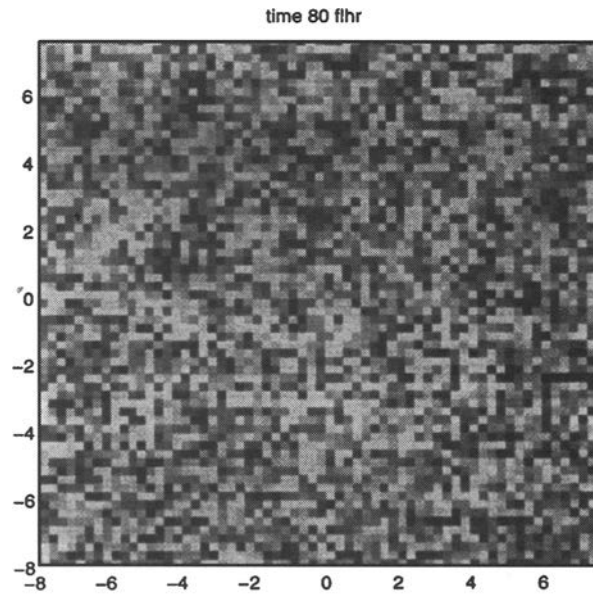
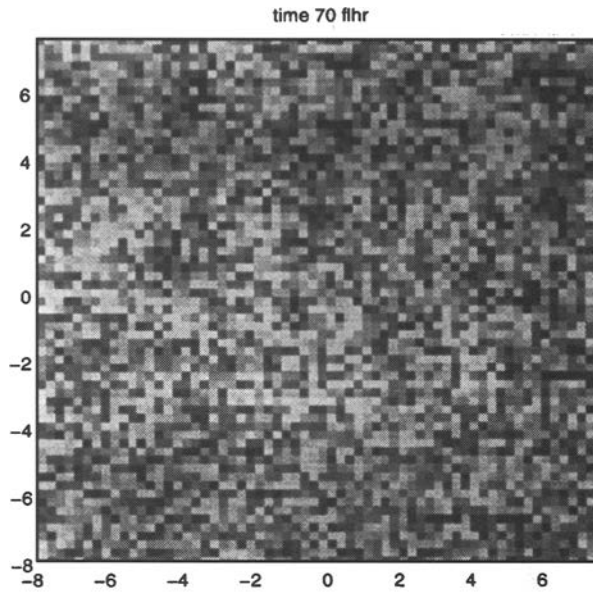


Figure 4. Tree health/MPB flight pattern on inhomogeneous forest with the same number of beetles emerging over 70, 80, 90 and 100 flight hours. Frame (a) shows the demographics of the forest when emergence occurs over a 70 flight hours period; light grey denotes high resin levels (good health); dark grey denotes lower resin level (poor health). There is no significant focusing of flying MPB at these emergence levels.

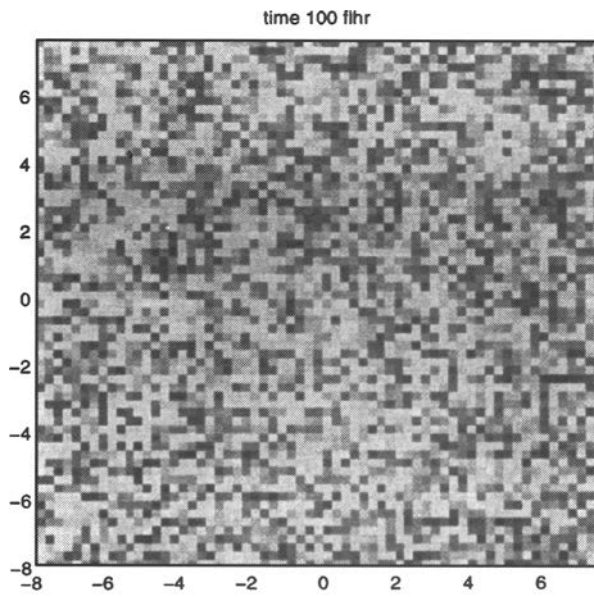
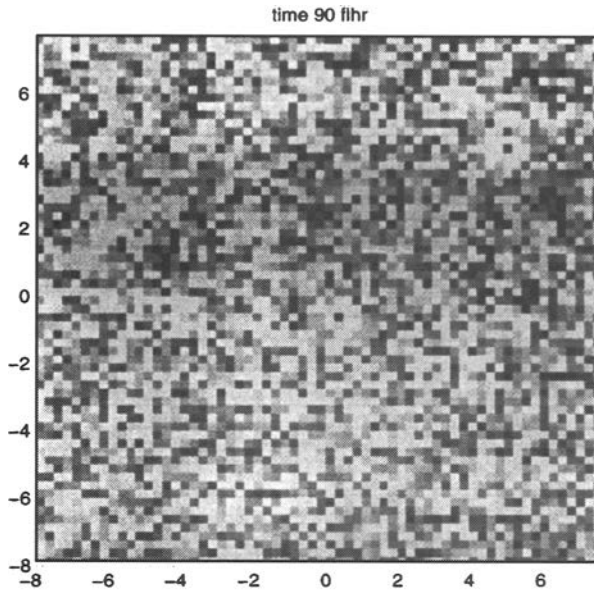


Figure 4. (Continued).

model indicates that synchronization of emergence plays an important role in the beetles ability to successfully engage in secondary attacks on trees of arbitrary health.

4.1. *Correlation between Q and R_0 .* In order to investigate the relationship between the original forest demographics and the pattern of infestation we look at the spatial correlation between Q and R_0 as a function of time. If \mathbf{u} and \mathbf{v} are n -vectors, then the means of the elements in \mathbf{u} and \mathbf{v} are

$$\bar{u} = \sum_{j=1}^n u_j/n \quad \text{and} \quad \bar{v} = \sum_{j=1}^n v_j/n,$$

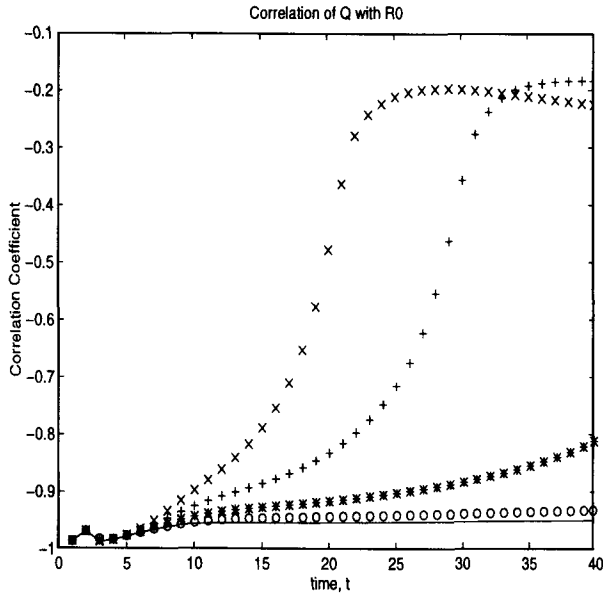
and the correlation coefficient between \mathbf{u} and \mathbf{v} is then given by

$$\text{corrcoef}(\mathbf{u}, \mathbf{v}) = \frac{\sum_{j=1}^n [(u_j - \bar{u})(v_j - \bar{v})]}{\sqrt{\sum_{j=1}^n [(u_j - \bar{u})^2] \sum_{j=1}^n [(v_j - \bar{v})^2]}}.$$

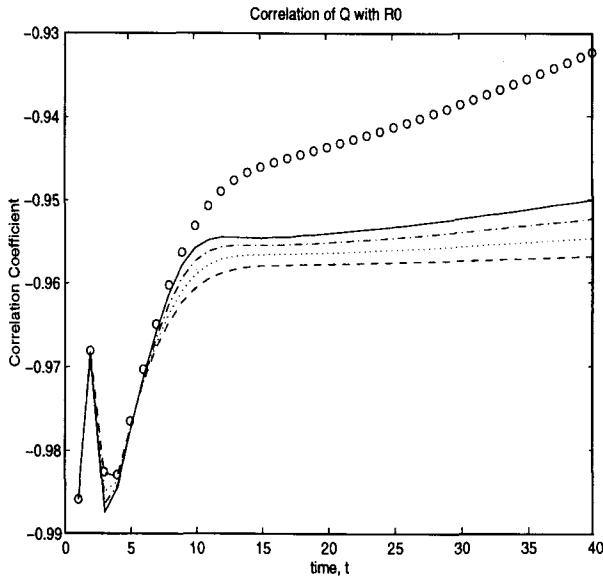
So the correlation between the two matrices, $Q(t)$ and R_0 , is the number $\text{corrcoef}(Q(t), R_0)$, where we view the matrices as long vectors. The correlation coefficient is a value between -1 and 1 , with -1 corresponding to an exact match in spatial pattern of low values of R_0 with high values of Q and with 1 being equivalent to $Q = kR_0 + c$ for some positive constants, k and c . The correlation coefficient is zero if there is no correlation in the spatial pattern of the matrix elements of Q and R_0 . When $\text{corrcoef}(Q(t), R_0)$ is close to -1 , the dispersal pattern is environmentally determined, meaning that the pattern of successful attack is almost completely determined by the pattern of weak trees in the forest.

Figure 5 is a graph of the correlation between Q and R_0 for different rates of emergence. The solid line corresponds to an emergence rate of 15 MPB/(hectare-flight hour) without chemotaxis. The other four lines in Fig. 5(a) correspond to emergence levels of 7.5, 10, 12.5 and 15 MPB/(hectare-flight hour) with chemotaxis. Figure 5(a) shows that at low levels of emergence, with chemotaxis, the infestation pattern has a strong negative correlation with the demographics of the forest and is almost identical to the correlation coefficient generated with environmental determinism. As the emergence rate increases there is a loss correlation, $\text{corrcoef}(Q(t), R_0)$ tends towards zero, which indicates the presence of successful secondary attacks against groups of trees independent of R_0 value.

Figure 5(b) shows one curve, with emergence of 7.5 MPB/(hectare-flight hour) and chemotaxis, indicated by the open circles and four curves at emergence levels of 7.5, 10, 12.5, and 15 MPB/(hectare-flight hour) with-



(a)



(b)

Figure 5. Correlation between peak health of the trees, R_0 , and infestation, Q . There are four levels of emergence with chemically directed moment; multiplication signs, $\gamma = 0.15$; pluses, $\gamma = 0.125$; asterisks, $\gamma = 0.1$; open circles, $\gamma = 0.075$. There are also four levels without chemical directed movement: solid line, $\gamma = 0.15$; dash-dot line, $\gamma = 0.125$; dotted line, $\gamma = 0.1$; dashed line, $\gamma = 0.075$. Part (a) is a comparison primarily of the correlation with chemotaxis, while (b) is primarily without chemotaxis.

out chemotaxis. In this case all five curves indicate a strong negative correlation between forest demographics and the corresponding patterns of attack. The only loss in negative correlation for the four lower curves can be attributed to the effects that A has on the conversion of flying MPB to nesting MPB. In this case of environmental determinism there is no successful switching from primary to secondary attacks as the emergence level is increased.

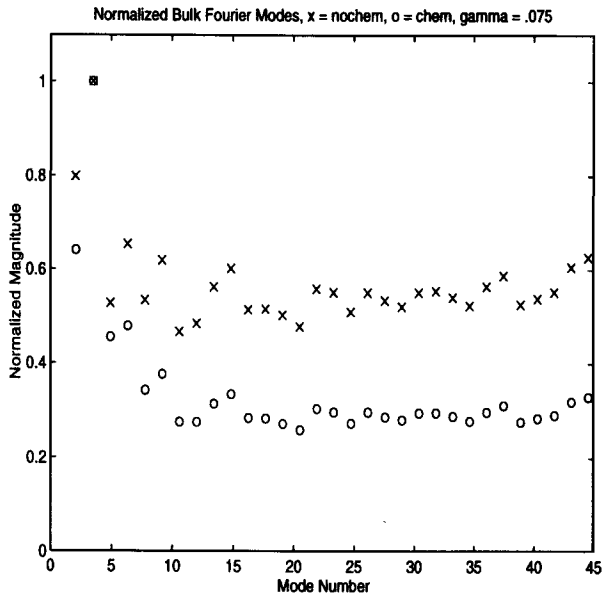
4.2. *Spectral comparison and change in scale.* Another way to show this marked difference in attack pattern between emergence levels with and without chemotaxis is to look at the spectrum of attack. Figure 6 shows the magnitudes of the bulk wave numbers for the spatial patterns of attack with chemotaxis (open circles) and without chemotaxis (multiplication signs) after 40 flight hours, at emergence levels of 7.5, 12.5 and 15 MPB/ (hectare-flight hour). These bulk wave numbers are an average of the magnitudes of waves of the same approximate wave length. If we write

$$Q_{jk} = \sum_{l=-n_x/2}^{n_x/2-1} \sum_{m=-n_y/2}^{n_y/2-1} \hat{Q}_{lm} \exp\left[\frac{\pi l x_j}{L_x} + \frac{\pi m y_k}{L_y}\right],$$

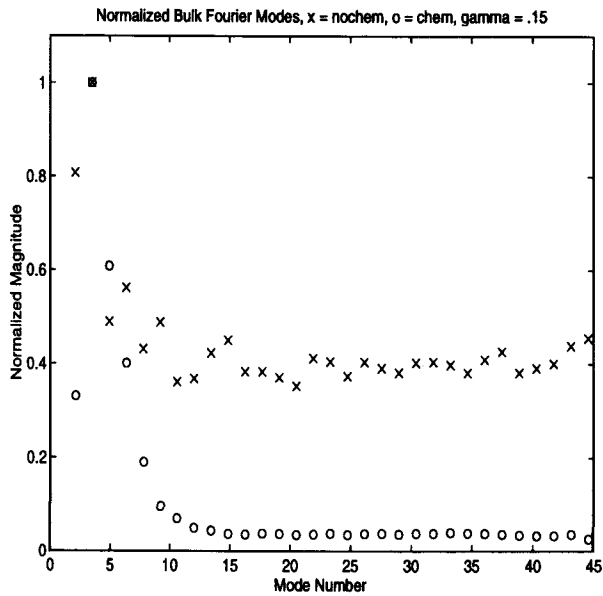
then the magnitude of the i th bulk wave number is the average of the magnitudes of \hat{Q}_{lm} for all l and m satisfying $i - \frac{1}{2} < \sqrt{l^2 + m^2} < i + \frac{1}{2}$. We then normalized each spectrum so that the largest mode has magnitude 1 to compare the resulting attack patterns with and without chemotaxis and with the demographics of the forest. In Fig. 6(a) we see the start of the characteristic bandwidth of attack with chemotaxis in the lower modes. However, the overall attack spectrum has the same shape both with and without chemically directed movement at this low level of emergence. Again this corresponds to the presence of only primary attacks on weak trees.

In Fig. 6(b) and (c) we see that at higher levels of emergence, the attack spectrum with chemotaxis is dominated by the lower modes while the non-chemotactic attacks maintain the same relative structure. In Fig. 6(c) we can compare the attack spectrum with the demographics of the forest. The plus signs represent the peak health spectrum of the trees. As expected, there is a strong correlation between the health spectrum and the spectrum of attack without chemotaxis.

In Fig. 6(d) we show the same results with a different randomly generated forest. Both Fig. 6(c) and (d) correspond with an emergence rate $\gamma = 0.125$, and the spectrum of attack with chemotaxis is the same in both cases, indicating the same pattern of secondary attacks. However, the spectra of attack without chemotaxis are not the same, but are correlated with the original demographics of the forest as expected.

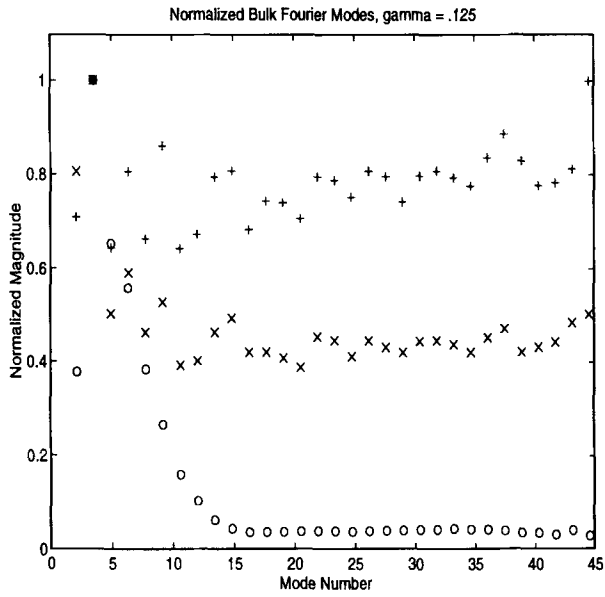


(a)

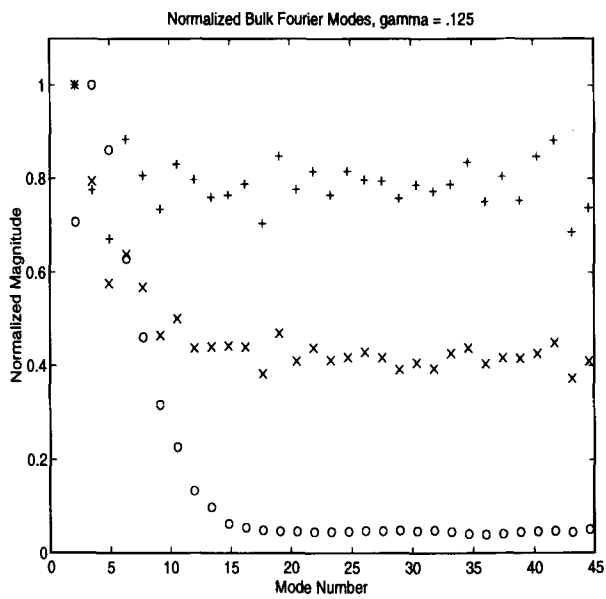


(b)

Figure 6. Normalized magnitudes of bulk wave numbers for infestation, Q , with (open circles) and without (multiplication signs) chemically directed movement. The pluses correspond to the spectrum of the forest, R_0 .



(c)



(d)

Figure 6. (Continued).

We have shown in Fig. 6(c) and (d) that changing the demographics of the forest does not change the statistical relationship of the attack patterns. To further validate our results we must also show that the attack relationship remain the same under a refinement of the numerical grid. In the above experiments we used a 64×64 numerical grid on a 1.6×1.6 km space domain. This gives a resolution of 25 m, so each grid point can represent several individual trees. Thus, as the resolution is increased, each grid point would be an average of characteristics of fewer trees. The obvious question is then: “do we get the same results at higher resolutions?”

To show that the attack patterns predicted by our model are independent of the grid size, we need to increase the resolution, maintain some degree of heterogeneity, insure that the same forest demographics are represented at both grid sizes and then compare patterns of attack. The only difficulty in increasing resolution is choosing R_0 . To generate R_0 s for a 64×64 and 128×128 grid point runs, we start by choosing random values between 0.5 and 1.5 for R_0 on a 32×32 grid, or a resolution of 50 m. We then refine R_0 from the 32×32 to a 64×64 grid using a nearest neighbor averaging scheme on all new grid points. To get the 128×128 grid of R_0 values, we refine the 64×64 grid again using nearest neighbor averaging on the new grid points. This method generates two resolutions of a forest where the heterogeneity is contained in the lowest 32 Fourier modes. This insures that there is no loss of high mode forcing when going from the 64×64 to the 128×128 simulation, while maintaining basically the same spatial demographics of the forest.

The clearest way to graphically compare the attack patterns at the two resolutions is to look at the correlations between Q and R_0 . In Fig. 7 we show the evolution of the $\text{corrcoef}(Q, R_0)$ over time at both a 25 and a 12.5 m resolution for simulations with chemotaxis at an emergence level of $\gamma = 0.125$. In both cases we see the same switching from primary to secondary attacks and that switching occurs at the same rate, with the same relative correlation values. We also observed the same pattern formations and spectra of attack in both simulations, but omit the corresponding pictures for brevity.

Based on these results, we are confident that our model demonstrates a statistically significant relationship between high rates of emergence and the MPB's ability to successfully participate in secondary attacks on trees of arbitrary health, a necessary component in an epidemic outbreak.

5. The Structure of Secondary Attack. In the previous sections we have shown that the model embodied in equations (1)–(6) exhibits a phase transition as the rate of emergence of flying MPB increases. The phase transition is indicated by a marked shift in correlation with environmental

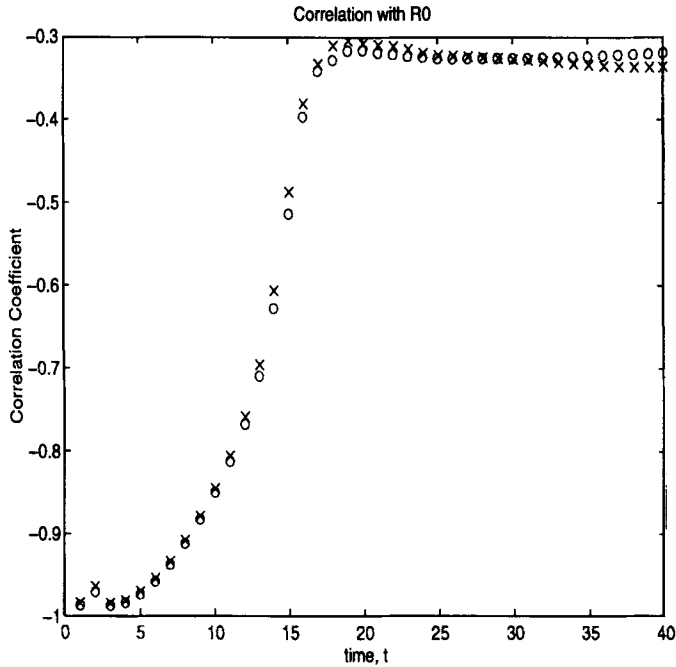


Figure 7. Correlation between peak health of the trees, R_0 , and infestation, Q , at two resolutions: open circles, 64×64 grid points; multiplication signs 128×128 grid points.

determining factors and change from broad and random to smooth spectral dispersal patterns. In this section we will demonstrate that the structure of dispersal after the phase transition is dominated by the success of *secondary* attacks. *Primary* attacks occur as MPB successfully nest in weak (low R_0) trees. Due to the combination of pheromone release and chemotaxis, the population of flying MPB responds with a motion of peak population levels away from the focus of the primary infestation. This is our model's rendition of the "switching" behavior reported by field observers. *Secondary* attacks occur when MPB have switched from the weak focus tree to potentially strong trees near the focus (Geizler *et al.*, 1980; Gara *et al.*, 1984). If successful, the pattern of trees infested after secondary attacks should be strongly correlated with the structure of the flying population's switching response. In this section we will analyze the asymptotic response of the model to successful point infestations, and show that the tail of the MPB spectrum obeys a distinctive power law. The exponent of this power law increases with the number of MPB nesting after a successful attack, and compares favorably with the numerical evidence. By contrast, before phase transition the spectrum of attacks has a spectrum precisely as broad as the randomly selected forest. From this we conclude that the pattern produced by epidemic infestation is dominated by the success of secondary attacks.

To begin with, we observe the parametric separation of scales. The parameters describing chemical movement a_j, b_j, δ_j are (at least) an order of magnitude greater than the parameters describing MPB dispersal μ, ν, κ . In turn the dispersal parameters are orders of magnitude larger than the remaining rate constants $r_j, r_3 \beta, \omega_j$. From these observations we may infer the following:

1. The chemical concentrations will rapidly come into equilibrium with respect to their (slowly varying) source terms.
2. The flying MPB response may be approximated as quasi-steady. That is, the chemical fields appearing in (4) will be constant on the time scales at which MPB respond, and the loss terms will be negligible when compared with the chemotactic responses.
3. After a successful attack, a focus tree's resin reservoir will be totally depleted, giving $R = 0$. Consequently the effect of equations (1)–(3) will be negligible in determining the switching behavior during a secondary attack, and the effect of C may be neglected.

These three observations will allow us to determine the population response at the time of switching.

We will assume

$$Q = q\delta(x)\delta(y),$$

where q is the number of MPB nesting in the focus tree after a successful primary attack. It would then seem natural to solve the steady-state version of (5) with delta-function forcing. Unfortunately, the solution has a logarithmic singularity at the primary infestation, which would make succeeding analysis untenable. Instead, we will model the chemical response as a Gaussian, and choose the shape parameters to be consistent with (5).

Define the moments M_0 and M_1 by

$$M_j \stackrel{\text{def}}{=} \int_0^\infty Ar^{j+1} dr.$$

Then, taking time derivatives and integrating by parts after substituting (5),

$$\frac{d}{dt}M_0 = a_1q - \delta_1M_0. \tag{10}$$

and

$$\frac{d}{dt}M_1 = b_1 \int_0^\infty A dr - \delta_1M_1. \tag{11}$$

If we require

$$A = 2 \frac{a}{\lambda^2} \exp\left[-\frac{r^2}{\lambda^2}\right],$$

then the steady solutions to (10) and (11) satisfy

$$a = \frac{a_1}{\delta_1} q$$

and

$$\frac{b_1}{\delta_1} a \frac{\sqrt{\pi}}{\lambda} = \frac{b_1}{\delta_1} \int_0^\infty A \, dr = M_1 = a \lambda \frac{\sqrt{\pi}}{2}.$$

This latter equation gives, in turn,

$$\lambda^2 = 2 \frac{b_1}{\delta_1}.$$

Hence, a Gaussian function which has the same first and second moment as the asymptotic pheromone response to a point infestation is

$$A_G \cong \frac{a_1 q}{b_1} \exp\left[-\frac{\delta_1 r^2}{2b_1}\right]. \tag{12}$$

Now we turn our attention to the quasi-steady MPB response to a given, stationary chemical signature. If we assume that the rate terms appearing in (4) are negligible at leading order, then the stationary response to chemical gradients satisfies

$$-\nabla[\nu P \nabla f(A, C) - \mu \nabla P] = 0. \tag{13}$$

Here

$$f(A, C) = A_3 \left[A_0 (A_3 + 1) \ln\left(\frac{A}{A_3 A_0} + 1\right) - A \right] + \frac{\kappa}{\nu} C.$$

For boundary conditions on (13), we require that P be finite at the origin and that

$$\lim_{r \rightarrow \infty} P = \frac{\gamma}{r_1 + \omega_1}.$$

This latter condition comes from requiring that asymptotic behavior of solutions to (13) be consistent with the steady-state asymptotic behavior of solutions to (4). The solution is given by

$$P_{qs}(r) = \frac{\gamma}{r_1 + \omega_1} \exp\left[\frac{\nu}{\mu} f(A_G(r), C = 0)\right]. \tag{14}$$

In Fig. 8 we compare the spectrum of nesting MPB from $\gamma = 0.125$ and 0.15 simulations on a randomly initialized forest with the spectrum of the theoretical secondary response, P_{qs} . Our rationale for the comparison is to determine how much of the structure of the dynamically dominated attack can be attributed to the success of secondary, switching attacks. The functional form of P_{qs} was parametrized using q values from the average surviving nesting beetles in focus trees (trees with $0.5 \leq R_0 \leq 0.6$). The agreement of spectra on the log-linear plot of Fig. 8 indicates that the computer simulations have power-law decay in their spectra, in spite of the broad-spectrum, random environment. This power-law decay agrees well with the power-law decay of the spectrum of MPB responding in secondary attacks. We may conclude that the small-scale structure of an epidemic is dominated by the success of secondary attacks. This is very much in agreement with published observations (Geizler *et al.*, 1980; Gara *et al.*, 1984).

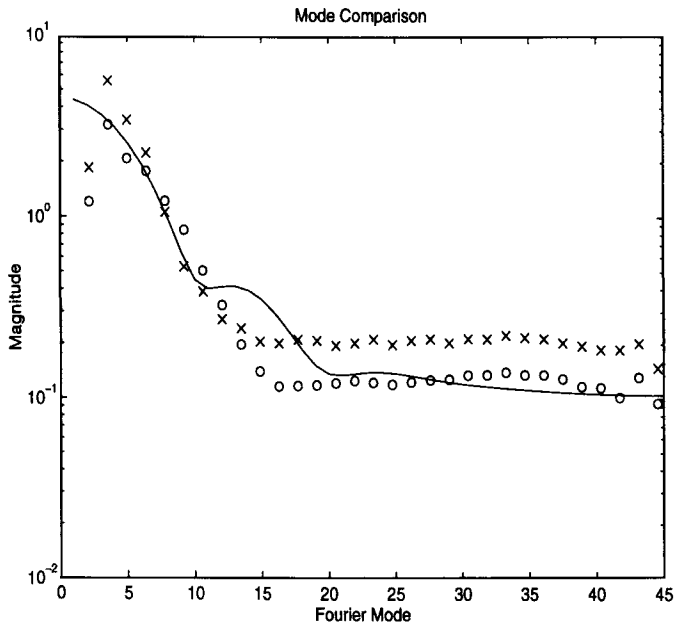


Figure 8. Comparison of asymptotic behavior: solid line, the spectrum of P_{qs} with numerical simulations; multiplication signs, $\gamma = 0.15$; open circles, $\gamma = 0.125$. The abscissa is plotted on a log scale so that the constant asymptotes of the spectral tails indicate similarities in power-law decay of k^{-1} .

6. Conclusions. In this paper we have presented a PDE model of the in-season dispersal of MPB, coupled with equations describing the interaction between the bark beetle and its host species. The model was constructed mechanistically as opposed to phenomenologically. That is, individual terms in all of the equations mathematically model components of MPB population behavior or aspects of pest/host interaction. The model was *not* built to have any particular global behavior, but was constructed with the intent of examining the landscape-scale consequences of various mechanistic processes in MPB dispersal. In our interactions with entomologists and ecologists, we have tried to view the mathematical model as a means of hypothesis testing. The various terms in the model are all mathematical descriptions of components of MPB/host dynamics which entomologists/ecologists hold to be relevant; the various parameters allow us to adjust the relative strength of those components. In this context, every selection of parameters, initial conditions and model integration is a particular example of examining the large-scale consequences of hypotheses about MPB dispersal.

With that in mind, we have had two goals in this paper. The first was to describe the mathematical model and our numerical approach to it, and the second was to examine the role of environmental determinism in outbreak initiation. To accomplish this latter goal we integrated the model with and without chemotaxis on a forest with randomly selected vigor (R_0). When the chemotactic terms are neglected (ν and κ set to zero), the only source of spatial structure is the explicit spatial variation of tree vigor. With chemotaxis operating (ν and κ non-zero), variations in R_0 still may affect the structure of the pattern. However, spatial patterns can also be generated dynamically, through the mechanism of pheromone self-focusing. We are thus selecting between two hypotheses on catastrophic outbreak phenomena: epidemic outbreaks are generated by chance propinquity of "weak" trees or epidemic outbreaks are caused by sufficiently large emergence of MPB.

The results presented in this paper indicate that the phase transition separating endemic from catastrophic epidemic behavior is mediated by increasing population levels. Our infestation pictures after phase transition are strongly reminiscent of the kill pattern in catastrophic MPB epidemics; the spotty infestation illustrated in the environmentally determined series of pictures is not observed in MPB outbreaks. It is clear that chance arrangement of weak trees serves to *seed* large-scale infestations, as is evidenced by the strong negative correlation initially between attacks and forest vigor. What characterizes spot eruption after the outbreak is the success of secondary attacks against trees of arbitrary vigor. Again, this is consistent with observations of incipient epidemics.

As modelers and applied mathematicians, these results are particularly satisfying to us, because phase transition behaviors were not built explicitly

into the model. We focussed our efforts on building faithful reflections of the mechanical, reductionistic aspects of MPB dispersal and host interactions. Consequently, we can view the mathematical and numerical results presented in this paper as tests of hypotheses in the sense discussed above. What we have demonstrated here is that the phase transition apparent in our model as population emergences increase is most strongly influenced by dynamic pattern formation and is less strongly influenced by environmental variability.

The authors are grateful for the generous support of the USDA Forest Service Mountain Pine Beetle Project [grants numbers INT-94904-CCSA (PW) and INT-94904-CCSA (JP)] and the NSF Division of Mathematical Sciences [grant number DMS-95-05327 (JP)]. We would also like to thank Jesse Logan and Barbara Bentz of the MPB Project and Rich Cutler of the Utah State University Statistics Consulting Center for many fruitful discussions.

REFERENCES

- Borden, J. H., L. C. Ryker, L. J. Chong, H. D. Pierce, B. D. Johnston and A. C. Oehlschlager. (1987). Response of the mountain pine beetle, *Dendroctonus ponderosae*, to five semiochemicals in British Columbia lodgepole pine forests. *Can. J. Forest. Res.* **17**, 118–128.
- Burden, R. L. and J. D. Faires. 1985. *Numerical Analysis*, 3rd ed. Boston: Prindle, Weber and Schmidt.
- Conn, J. E., J. H. Borden, B. E. Schott, L. M. Friskie, H. D. Pierce and A. C. Oehlschlager. 1983. Semiochemicals for the mountain pine beetle, *Dendroctonus ponderosae*, in British Columbia: field trapping studies. *Can. J. Forest. Res.* **13**, 320–324.
- Gara, R. I., D. R. Geiszler and W. R. Littke. 1984. Primary attraction of the mountain pine beetle to lodgepole pine in Oregon. *Ann. Entomol. Soc. Am.* **77**, 333–334.
- Gear, C. W. 1971. *Numerical Initial Value Problems in Ordinary Differential Equations*. Englewood Cliffs, NJ: Prentice-Hall.
- Geiszler, D. R., V. F. Gallucci and R. I. Gara. 1980. Modeling the dynamics of mountain pine beetle aggregation in a lodgepole pine stand. *Oecologia* **46** 244–253.
- Geiszler, D. R. and R. I. Gara. 1978. Mountain pine beetle attack dynamics in lodgepole pine. In *Theory and Practice of Mountain Pine Beetle Management in Lodgepole Pine Forests: Symp. Proc.*, A. A. Berryman, G. D. Amman and R. W. Stark (Eds). Pullman, WA: Washington State Univ.
- Hughes, P. R. 1973. *Dendroctonus*: production of pheromones and related compounds in response to host monoterpenes. *Zeit. Angew. Ent.* **73**, 294–312.
- Hunt, D. W. A., J. H. Borden, B. S. Lindgren and G. Gries. 1989. The role of autoxidation of alpha pinene in the production of pheromones of *Dendroctonus ponderosae*. *Can. J. Forest. Res.* **19**, 1275–1282.
- Hynum, B. G. and A. A. Berryman. 1980. *Dendroctonus ponderosae* (Coleoptera: Scolytidae): preaggregation landing and gallery initiation on lodgepole pine. *Can. Entomol.* **112**, 185–191.
- McCambridge, W. F. 1967. Nature of induced attacks by the black hills beetle, *Dendroctonus ponderosae* (Coleoptera: Scolytidae). *Ann. Entomol. Soc. Am.* **60**, 920–928.
- Moeck, H. A. and C. S. Simmons. 1991. Primary attraction of mountain pine beetle to bolts of lodgepole pine. *Can. Entomol.* **123**, 299–304.

- Nebeker, T. E., J. D. Hodges and C. A. Blanche. 1993. Host responses to bark beetle pathogen colonization. In *Beetle-Pathogen Interactions in Conifer Forests*, T. D. Schowalter and G. M. Filip (Eds). New York: Academic Press.
- Norris, D. M. and J. E. Baker. 1967. Feeding response of *Scolytus* to chemical stimuli in the bark of *Ulmus*. *J. Insect Phys.* **13**, 955–962.
- Pitman, G. B. 1971. Trans-verbenol and alpha-pinene: their utility in manipulation of the mountain pine beetle. *J. Econ. Entomol.* **64**, 426–430.
- Pitman, G. B., J. P. Vite, G. W. Kinzer and A. F. Fentiman. 1968. Bark beetle attractants: trans-verbenol isolated from *Dendroctonus*. *Nature* **218**, 168–169.
- Powell, J. A. and J. D. Rose. 1996. Local consequences of a global model for mountain pine beetle mass attack. *Dynamics Stability Syst.* **12**.
- Powell, J., J. A. Logan and B. J. Bentz. 1995. Local projection of a global model of mountain pine beetle attacks. *J. Theoret. Biol.* **179**, 243–260.
- Press, W. H., W. T. Vetterling, S. A. Teukolsky and B. P. Flannery. 1992. *Numerical Recipes in C*, 2nd ed. London: Cambridge Univ. Press.
- Prokopy, R. J. 1980. Epidectic pheromones influencing spacing patterns of phytophagous insects. In *Semiochemicals: Their Role in Pest Control*, D. A. Norlund, R. L. Jones and W. J. Lewis (Eds). New York: Wiley.
- Raffa, K. F. 1988. Host orientation behavior of *Dendroctonus ponderosae*: integration of token stimuli and host defenses. In *Mechanism of Woody Plant Resistance to Insects and Pathogens*, W. J. Mattson, J. Levieux and C. Bernard-Dagen (Eds), pp. 369–390. New York: Springer-Verlag.
- Raffa, K. F. and A. A. Berryman. 1979. Flight responses and host selection by bark beetles. In *Dispersal of Forest Insects: Evaluation, Theory and Management Implications*, A. A. Berryman and L. Safranyik (Eds), pp. 213–233. Pullman, WA: Washington State University.
- Raffa, K. F., T. W. Phillips and S. M. Salom. 1993. Strategies and mechanisms of host colonization by bark beetles. In *Beetle-Pathogen Interactions in Conifer Forests*, T. D. Schowalter and G. M. Filip (Eds), pp. 103–120. New York: Academic Press.
- Raffa, K. F. and A. A. Berryman. 1982. Gustatory cues in the orientation of *Dendroctonus ponderosae* (Coleoptera: Scolytidae) to host trees. *Can. Entomol.* **114**, 97–104.
- Raffa, K. F., T. W. Phillips and S. M. Salom. 1993. Strategies and mechanisms of host colonization by bark beetles. In *Beetle-Pathogen Interactions in Conifer Forests*, T. D. Schowalter and G. M. Filip (Eds), pp. 103–120. New York: Academic Press.
- Rasmussen, L. A. 1974. Flight and attack behavior of mountain pine beetle in lodgepole pine of northern Utah and southern Idaho. Research Note INT-18, USDA Forest Service.
- Reid, R. W., H. S. Whitney and J. A. Watson. 1967. Reactions of lodgepole pine to attack by *Dendroctonus ponderosae hopkins* and blue stain fungi. *Can. J. Botany* **45**, 1115–1116.
- Renwick, J. A. A. and J. P. Vite. 1970. Systems of chemical communication in *Dendroctonus*. *Contrib. Boyce Thompson Inst.* **23**, 355–360.
- Roe, A. L. and G. D. Amman. 1970. The mountain pine beetle in lodgepole pine forests. Research Paper INT-71, USDA Forest Service.
- Safranyik, L., R. Silversides, L. H. McMullen and D. A. Linton. 1989. An empirical approach to modeling the local dispersal of the mountain pine beetle (*Dendroctonus ponderosae hopk.*) in relation to sources of attraction, wind direction and speed. *J. Appl. Entomol.* **108**, 498–511.
- Schmitz, R. F. 1988. Understanding Scolytid problems in lodgepole pine forests: the need for an integrated approach. In *Integrated Control of Scolytid Bark Beetles*, T. L. Payne and H. Saarenmaa (Eds). Blacksburg, VA: Virginia Polytechnic Institute and State University.
- Schonherr, J. 1976. Mountain pine beetle: visual behavior related to integrated control. In *Proceedings, XVI IUFRO World Congress, Oslo, Norway*, pp. 449–452.
- Schowalter, T. D. and G. M. Filip (Eds). 1993. *Beetle-Pathogen Interactions in Conifer Forests*. New York: Academic Press.
- Sheppard, R. F. 1966. Factors influencing the orientation and rates of activity of *Dendroctonus ponderosae* (Coleoptera: Scolytidae). *Can. Entomol.* **98**, 507–518.

- Smith, R. H. 1963. Toxicity of pine resin vapors to three species of *Dendroctonus* bark beetles. *J. Econ. Entomol.* **56**, 827–831.
- Smith, R. H. 1966. Resin quality as a factor in the resistance of pines to bark beetles. In *Proceedings of the NATO and National Science Foundation*, H. D. England, R. E. Gerhold, R. E. McDermot, E. J. Schreiner and J. A. Winieski (Eds), pp. 189–196. Oxford, England: Pergamon.
- Tkacz, B. M. and R. F. Schmitz. 1986. Association of an endemic mountain pine beetle population with lodgepole pine infected by *Armillaria* root disease in Utah. Research Note INT-353, USDA Forest Service.
- White, P. and J. Powell. 1996. Spatial invasion of pine beetles into lodgepole forests: a numerical approach. Unpublished manuscript.
- Wood, D. L. 1972. Selection and colonization of ponderosa pine by bark beetles. *Symp. Roy. Entomol. Soc. London* **6**, 110–117.

Received 22 July 1996

Revised version accepted 17 December 1996